

Optimization and Control Analysis of a Multi-Phase Buck Converter Utilizing MOSFETs

Dobroslav Kovac, Irena Kovacova

Technical University of Kosice, 042 00, Slovak Republic
e-mail: dobroslav.kovac@tuke.sk

Abstract. The study explores the design, optimization, and application of a control strategy tailored for a multi-phase buck converter employed to manage energy processing from photovoltaic panel. A control method is proposed to maximize the energy conversion efficiency. It is grounded in a comprehensive examination of the converter switching dynamics, factoring in significant parasitic elements of the circuit and the operational traits of power semiconductor devices, specifically MOSFETs. The method effectiveness and precision are validated by computational simulations and experimental measurements conducted on an actual photovoltaic system utilizing a particular converter type. The method is adaptable to various multi-phase converter configurations and alternative power semiconductor devices.

Keywords: multi-phase DC-DC power converters, synthesis of optimal control, power measurement, energy efficiency, photovoltaic systems

Optimizacija in analiza krmiljenja večfaznega pretvornika navzdol s tranzistorji MOSFET

Študija obravnava zasnovano, optimizacijo in uporabo krmilne strategije, prilagojene za večfazni pretvornik navzdol, ki se uporablja za upravljanje pretoka energije iz fotonapetostne plošče. Predlagana je krmilna metoda, katere cilj je maksimirati učinkovitost pretvorbe energije. Temelji na temeljiti analizi stikalne dinamike pretvornika, pri čemer so upoštevani pomembni parazitski elementi vezja in obratovne lastnosti močnostnih polprevodniških komponent, zlasti tranzistorjev MOSFET.

Učinkovitost in natančnost metode sta potrjeni s pomočjo računalniških simulacij in eksperimentalnih meritev, izvedenih na dejanskem fotonapetostnem sistemu, ki uporablja določen tip pretvornika. Metoda je prilagojena različnim konfiguracijam večfaznih pretvornikov in alternativnim močnostnim polprevodniškim elementom.

1 INTRODUCTION

Multi-phase converters provide several benefits over single-phase designs in photovoltaic panel applications [1-5]. Their benefits are a higher energy transfer efficiency due to the absence of interruptions in the energy flow, reduced output current ripple, narrow ranges of discontinuous currents, and the possibility of operating at low switching frequencies for individual transistors [6-8]. However, multi-phase converters also present notable challenges when compared to single-phase configurations. The main among them is an increased complexity of the circuit resulting in a higher

component count, greater cumulative losses, and diminished overall efficiency. To mitigate the drawbacks and enhance the efficiency, an adaptive control method is employed which dynamically adjusts the converter topology by modifying the number of the active switching phases in response to the variations in the input power.

2 CONVERTER DESIGN AND ANALYSIS OF ITS LOSSES

Fig. 1a) shows a schematic diagram of a multi-phase buck converter employed for energy conversion in systems such as photovoltaic panels [9-13]. Fig. 1b) provides a detailed depiction of the converter, explicitly highlighting its parasitic components. The circuit elements are marked with subscript "P" which represents parasitic characteristics. According to the Kirchhoff's law, the currents in the circuit are governed by the relationship expressed in (1).

$$i = \sum_{j=1}^n i_j \quad (1)$$

The operation of the converters phases is synchronized with switching signals for each phase offset by a time interval of T/n , where T is the switching period and n is the total number of phases. The functioning of each phase can be categorized into two primary intervals.

Received: 18 December 2024

Accepted: 15 April 2025



Copyright: © 2025 by the authors.
Creative Commons Attribution 4.0
International License

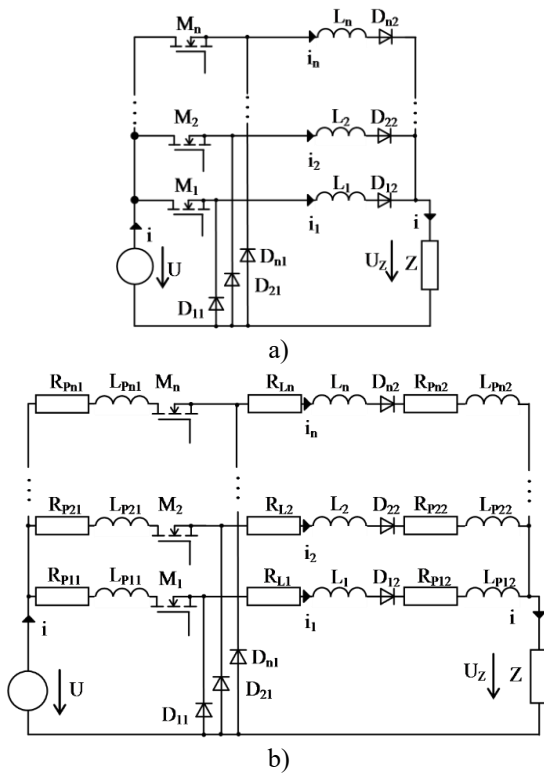


Figure 1. a) Schematic diagram of an n -phase buck converter, b) detailed diagram of an n -phase converter with its parasitic components.

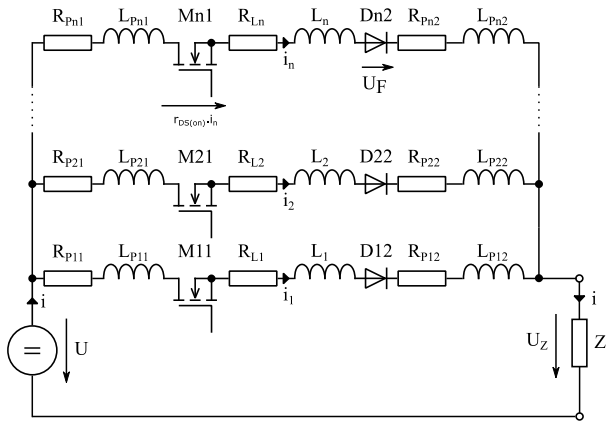


Figure 2. Equivalent circuit diagram for the converter first operating interval.

1. interval - switch M closed

During the operational interval, transistor M in the respective phase remains off, allowing the energy to flow from voltage source U through the circuit primary inductance L to the load (See Fig. 2).

The relationship governing the n -th loop of the converter is expressed mathematically as:

$$-U + R_{Pn1} \cdot i_n + L_{Pn1} \cdot \frac{di_n}{dt} + r_{DS(on)n} \cdot i_n + R_{Ln} \cdot i_n + L_n \cdot \frac{di_n}{dt} + U_F + R_{Pn2} \cdot i_n + L_{Pn2} \cdot \frac{di_n}{dt} + U_Z = 0 \quad (2)$$

where U is the input voltage, R_{Pn1} the resistance of the input conductor, L_{Pn1} the parasitic inductance of the input conductor, and $r_{DS(on)}$ the on-state resistance of the MOSFET transistor, R_{Ln} is the resistance of the main

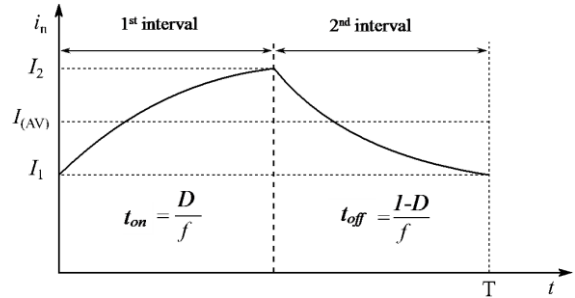


Figure 3. Current waveform in the n th phase.

coil, L_n is the inductance of the main coil, U_F is the voltage drop across the diode, R_{Pn2} is the resistance of the conductor leading to the load, and U_Z is the voltage at the load. As the circuit comprises only a resistive-inductive load, the current waveform takes the shape shown in Fig. 3. The converter loop of the n -th phase can be simplified through parameter concentration.

$$U_Z = Z \cdot I = Z \cdot \sum_{j=1}^n i_j \approx Z \cdot n \cdot i_n \quad (3)$$

$$U_F = U_{TO} + r_F \cdot i_n \quad (4)$$

$$R_{n1} = R_{Pn1} + r_{DS(on)} + R_{Ln} + r_F + R_{Pn2} \quad (5)$$

$$L_{n1} = L_{Pn1} + L_n + L_{Pn2} \quad (6)$$

Where U_{TO} is the threshold voltage of the diode, R_{n1} is the resistance of the n -th phase during the first interval, r_F is the forward resistance of the diode, and L_{n1} is the inductance of the n -th phase during the first interval. By incorporating equations (3) to (6), equation (2) can be reformulated as follows:

$$U_{TO} - U + Z \cdot n \cdot i_n + R_{n1} \cdot i_n + L_{n1} \cdot \frac{di_n}{dt} = 0 \quad (7)$$

The equation rewritten in the operator form using the Laplace-Carson transform is:

$$U_{TO} - U + Z \cdot n \cdot \hat{i}_n + R_{n1} \cdot \hat{i}_n + pL_{n1} \cdot \hat{i}_n - pL_{n1} \cdot I_1 = 0 \quad (8)$$

The relationship describing the desired current waveform derived from equation (8) is:

$$\hat{i}_n = \frac{U - U_{TO}}{(R_{n1} + n \cdot Z)} \cdot \frac{L_{n1}}{(R_{n1} + n \cdot Z) + p} + I_1 \cdot \frac{p}{(R_{n1} + n \cdot Z) + p} \quad (9)$$

Applying the inverse transform to return to the time domain gives:

$$i_n = \frac{U - U_{TO}}{(R_{n1} + n \cdot Z)} \left(1 - e^{-\frac{(R_{n1} + n \cdot Z) \cdot t}{L_{n1}}} \right) + I_1 \cdot e^{-\frac{(R_{n1} + n \cdot Z) \cdot t}{L_{n1}}} \quad (10)$$

By substituting $t = t_{on}$ with D/f in the time-domain expression for the current, the input current corresponds to I_2 (See Fig. 3).

$$I_2 = \frac{U - U_{TO}}{(R_{n1} + n \cdot Z)} \left(1 - e^{-\frac{(R_{n1} + n \cdot Z) \cdot D}{L_{n1} \cdot f}} \right) + I_1 \cdot e^{-\frac{(R_{n1} + n \cdot Z) \cdot D}{L_{n1} \cdot f}} \quad (11)$$

Where D is a duty cycle of the converter control and f is its switching frequency.

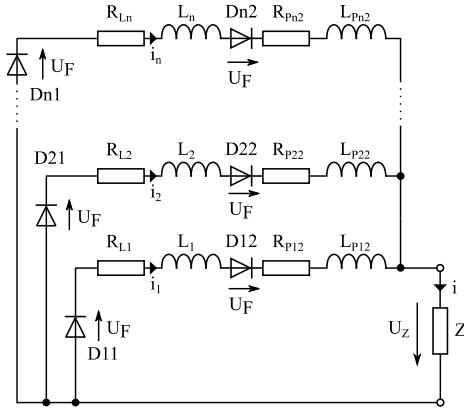


Figure 4. Equivalent circuit diagram for the second operating interval of the converter.

II. interval - switch M turned off

During the interval, the energy stored in inductance L_n is delivered to the load via diodes D_{n1} and D_{n2} (See Fig. 4). The equation representing the n -th loop of the converter is expressed as follows:

$$U_Z + U_F + R_{Ln} \cdot i_n + L_n \cdot \frac{di_n}{dt} + U_F + R_{Pn2} \cdot i_n + L_{Pn2} \cdot \frac{di_n}{dt} = 0 \quad (12)$$

The formulation adheres to equations (3) and (4), along with the following additional relationships:

$$R_{n2} = R_{Ln} + 2 \cdot r_F + R_{Pn2} \quad (13)$$

$$L_{n2} = L_n + L_{Pn2} \quad (14)$$

Substituting their values into equation (12) gives:

$$n \cdot Z \cdot i_n + 2 \cdot U_{TO} + R_{n2} \cdot i_n + L_{n2} \cdot \frac{di_n}{dt} = 0 \quad (15)$$

It is resolved using the operator form:

$$n \cdot Z \cdot \hat{i}_n + 2 \cdot U_{TO} + R_{n2} \cdot \hat{i}_n + p L_{n2} \cdot \hat{i}_n - p L_{n2} \cdot I_2 = 0 \quad (16)$$

The desired current is then derived as:

$$\hat{i}_n = \frac{-2U_{TO}}{(R_{n2} + n \cdot Z)} \cdot \frac{L_{n2}}{(R_{n2} + n \cdot Z) + p} + I_2 \cdot \frac{p}{(R_{n2} + n \cdot Z) + p} \quad (17)$$

Using an inverse transformation, the time-dependent behavior of the desired current is:

$$i_n = \frac{-2U_{TO}}{(R_{n2} + n \cdot Z)} \left(1 - e^{-\frac{(R_{n2} + n \cdot Z) \cdot t}{L_{n2}}} \right) + I_2 \cdot e^{-\frac{(R_{n2} + n \cdot Z) \cdot t}{L_{n2}}} \quad (18)$$

By substituting $t = t_{off} = (1-D)/f$, the expression for the input current of magnitude I_1 is derived (See Fig. 3):

$$I_1 = \frac{-2U_{TO}}{(R_{n2} + n \cdot Z)} \left(1 - e^{-\frac{(R_{n2} + n \cdot Z) \cdot (1-D)}{L_{n2} \cdot f}} \right) + I_2 \cdot e^{-\frac{(R_{n2} + n \cdot Z) \cdot (1-D)}{L_{n2} \cdot f}} \quad (19)$$

Using equations (11) and (19), the expressions for the initial values of currents I_1 and I_2 at the start of both converter intervals are derived. They depend solely on the circuit parameters. By substituting value I_2 from equation (11) into equation (19), the following relationship is obtained:

$$I_1 = \frac{-2U_{TO}}{(R_{n2} + n \cdot Z)} \left(1 - e^{-\frac{(R_{n2} + n \cdot Z) \cdot (1-D)}{L_{n2} \cdot f}} \right) + \frac{\left(\frac{U - U_{TO}}{(R_{n1} + n \cdot Z)} \left(1 - e^{-\frac{(R_{n1} + n \cdot Z) \cdot D}{L_{n1} \cdot f}} \right) \cdot e^{-\frac{(R_{n2} + n \cdot Z) \cdot (1-D)}{L_{n2} \cdot f}} \right)}{\left(1 - e^{-\frac{(R_{n1} + n \cdot Z) \cdot D}{L_{n1} \cdot f}} \cdot e^{-\frac{(R_{n2} + n \cdot Z) \cdot (1-D)}{L_{n2} \cdot f}} \right)} \quad (20)$$

The value of current I_2 is determined by substituting equation (19) into equation (11):

$$I_2 = \frac{U - U_{TO}}{(R_{n1} + n \cdot Z)} \left(1 - e^{-\frac{(R_{n1} + n \cdot Z) \cdot D}{L_{n1} \cdot f}} \right) + \frac{-2U_{TO}}{(R_{n2} + n \cdot Z)} \left(1 - e^{-\frac{(R_{n2} + n \cdot Z) \cdot (1-D)}{L_{n2} \cdot f}} \right) + \frac{\left(\frac{U - U_{TO}}{(R_{n1} + n \cdot Z)} \left(1 - e^{-\frac{(R_{n1} + n \cdot Z) \cdot D}{L_{n1} \cdot f}} \right) \cdot e^{-\frac{(R_{n2} + n \cdot Z) \cdot (1-D)}{L_{n2} \cdot f}} \right)}{\left(1 - e^{-\frac{(R_{n1} + n \cdot Z) \cdot D}{L_{n1} \cdot f}} \cdot e^{-\frac{(R_{n2} + n \cdot Z) \cdot (1-D)}{L_{n2} \cdot f}} \right)} \cdot e^{-\frac{(R_{n1} + n \cdot Z) \cdot D}{L_{n1} \cdot f}} \quad (21)$$

Using equations (10), (18), (20), and (21), the time evolution of the current in any phase of a multi-phase buck converter is calculated. To determine the optimal number of the converter phases, the losses associated with the varying phase configurations are assessed. They occur both during a steady-state operation, encompassing both intervals of the operation, and during transient processes. The loss components and corresponding designations are:

Steady-state losses:

- P_{RPn1} are the losses resulting from the resistance of the supply line in the n-th phase,
- P_{MF} are the losses occurring when the MOSFET transistor is in the switched-on state,
- P_{MR} are the losses occurring when the MOSFET transistor is in the switched-off state,
- P_{RLn} are the losses associated with the resistance of the coil in the n-th phase,
- P_{DF} are to the losses occurring when the diode is in the switched-on state,
- P_{DR} are the losses occurring when the diode is in the switched-off state,
- P_{RPn2} are the losses caused by the resistance of the supply conductors to the load in the n-th phase.

Transient losses:

- P_{Mon} are the MOSFET switching-on losses,
- P_{Moff} are the MOSFET switching-off losses,
- P_{DQR} are the diode switching-off losses,
- P_{DQF} are the diode switching-on losses.

Taking into account the standard turn-on and turn-off waveforms and equation (1), the total P_C losses of the converter are:

$$P_C = P_{RPn1} + P_{MF} + P_{MR} + P_{RLn} + P_{DF} + P_{DR} + P_{RPn2} + P_{Mon} + P_{Moff} + P_{DQR} + P_{DQF} \quad (22)$$

The average phase current of the converter is calculated using equation (23).

$$I_{n(AV)} = \frac{I_1 + I_2}{2} = \frac{I}{n} \quad (23)$$

The total losses in the converter are then expressed as:

$$P_C = nR_{Pn1}I_{n(AV)}^2D + nr_{DS(on)}I_{n(AV)}^2D + nUI_{DS(off)}(1-D) + nR_{Ln}I_{n(AV)}^2 + n2(U_{TO} + r_F I_{n(AV)})I_{n(AV)}(1-D) + n(U_{TO} + r_F I_{n(AV)})I_{n(AV)}D + nUI_R D + nR_{Pn2}I_{n(AV)}^2 + n\frac{1}{2}UI_1t_{on}f + n\frac{1}{2}UI_2t_{off}f + n\frac{1}{2}Q_{rr}Uf + n\frac{1}{2}U_{FP}I_2t_{fr}f \quad (24)$$

Where $r_{DS(on)}$ is the on-state resistance of the transistor, I_R is the reverse current through the diode, $I_{DS(off)}$ is the current through the transistor during its turn-off period, t_{on} is the turn-on time of the MOSFET transistor, t_{off} is the turn-off time of the MOSFET transistor, Q_{rr} is the reverse recovery charge of the diode, and U_{FP} is the voltage across the diode during its transition from the off state to the on state. The transition duration is defined by t_{fr} . By simplifying equation (24) using the relationships in equation (23), a simplified form of the expression is obtained.

$$P_C = \left(\frac{I^2}{n}\right) \left(R_{Pn1}D + r_{DS(on)}D + R_{Ln} + 2r_F(1-D) + r_FD + R_{Pn2} \right) + nUI_{DS(off)}(1-D) + 2U_{TO}I(1-D) + U_{TO}ID + nUI_R D + n\frac{1}{2}UI_1t_{on}f + n\frac{1}{2}UI_2t_{off}f + n\frac{1}{2}Q_{rr}Uf + n\frac{1}{2}U_{FP}I_2t_{fr}f \quad (25)$$

The converter efficiency is expressed using equation (26):

$$\eta = \frac{P_{output}}{P_{input}} = \frac{P_{input} - P_C}{P_{input}} \quad (26)$$

Equation (26) shows that the overall efficiency is primarily affected by the total power losses. They can be reduced by using design components. The total losses are also affected by the number of parallel phases in the converter. As the input current is distributed linearly across the phases, the losses in the phase resistors decrease quadratically. Therefore, using multiple phases may result in lower total losses compared to a single-phase configuration. However, due to the additional losses in the parallel phases, the assumption that increasing the number of the phases always reduces the losses is not entirely accurate. It is therefore possible to determine the optimal number of phases for a specific input power. The converters efficiency at any given input power can be maximized by adjusting its topology and duty cycle, while considering the fixed design parameters and characteristics of the converter components. By differentiating equation (25) for the P_C power losses with respect to the number of phases n , the optimal phase count that minimizes power losses can be determined at any point during the converters operation.

$$n = I \sqrt{\frac{R_{Pn1}D + r_{DS(on)}D + R_{Ln} + 2r_F(1-D) + r_FD + R_{Pn2}}{UI_{DS(off)}(1-D) + UI_R D + 0.5f(U_1t_{on} + UI_2t_{off} + Q_{rr}U + U_{FP}I_2t_{fr})}} \quad (27)$$

Equation (27) shows that depending on the converters design and its instantaneous power input, the optimal number of the controlled phases in a multi-phase buck converter to minimize the power losses is obtained. However, implementing such control requires a microcontroller with a significant computational power

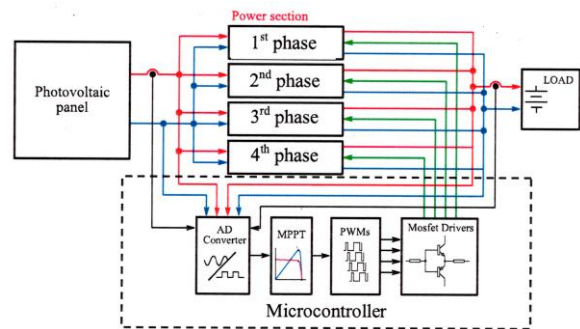


Figure 5. Schematic diagram of the designed four phase buck converter.

and access to static and dynamic parameters of the components involved, which can be a demanding task. A simpler approach is to measure the converters efficiency in real time and adjust the number of active phases accordingly. Fig. 5 shows the proposed circuit and its supplementary circuits [14-19] of the tested four phase buck converter commonly used in photovoltaic energy conversion.

High-speed MOSFET transistors are employed as the switching elements in the converter. Fig. 6 shows a practical implementation of the four phase converter prototype.



Figure 6. Practical implementation of the converter prototype.

For the converter to operate correctly, precise control signals at switching frequency f are required. They must be time-shifted by interval $t = T/n$, where n is the number of switching phases. Their duration must be adjustable based on duty cycle D varying from 0 to 1. The signals are generated using the microcontroller in the control section of the circuit (See Fig. 5). For this purpose, a NUCLEO-F746ZG development board, equipped with an adequate microcontroller, is used. A preview of the development board is presented in Fig. 7. The microcontroller consists of three 12-bit analog-to-digital converters capable of processing signals from sensors and supporting up to 24 analog channels.

Fig. 8 shows an example of the generated control signals with a duty cycle of $D = 0.2$.

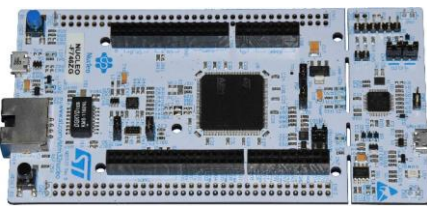


Figure 7. NUCLEO-F746ZG Development Board.

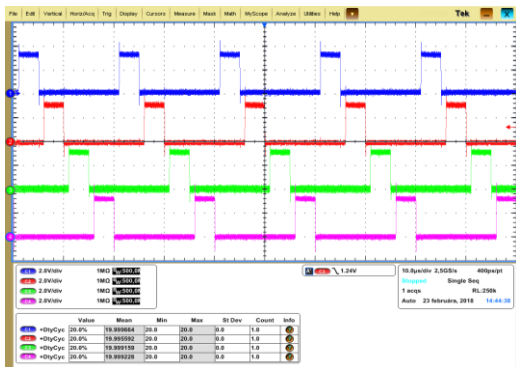


Figure 8. Control signals for MOSFETs generated by the microcontroller, C1: 2V/div is 1st phase, C2: 2V/div is 2nd phase, C3: 2V/div is 3rd phase, C4: 2V/div is 4th phase, time is 10 μ s/div.

Figs. 9 and 10 show the output waveforms of the converter operating in single-phase and three-phase modes. Analyzing the waveforms proves the advantageous characteristics of the multi-phase operation.

The verification of the efficiency of a multi-phase converter does not depend only on its power input but also on the number of active phases the converter is analyzed using computer simulations and practical measurements. The verification results of the analyses are presented in Figs. 11 and 12.

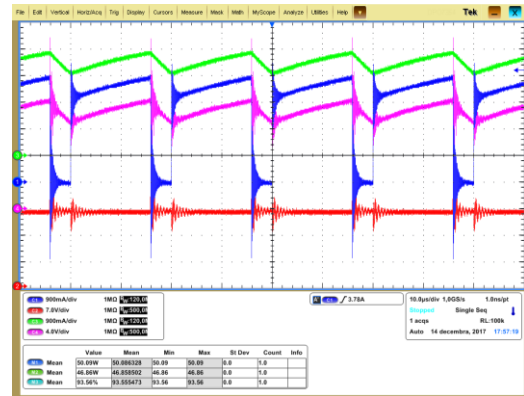


Figure 9. Measured voltage and current waveforms of a single-phase buck converter at the input power of 50W, C1: 900mA / div is the input current, C2: 7V / div is the input voltage, C3: 900mA / div is the output current, C4: 4V / div is the output voltage, M1 is the mean value of the input power, M2 is the mean value of the output power, M3 is the mean value of the efficiency.

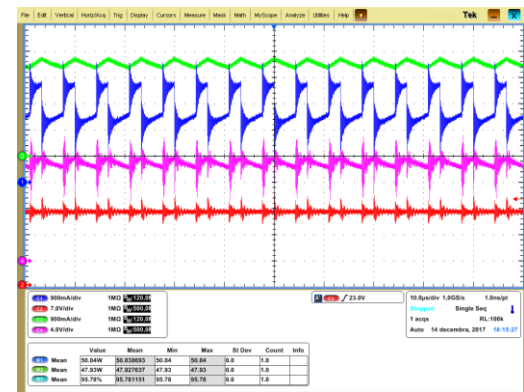


Figure 10. Measured voltage and current waveforms of a three-phase buck converter at the input power of 50W, C1: 900mA / div is the input current, C2: 7V / div is the input voltage, C3: 900mA / div is the output current, C4: 4V / div is the output voltage, M1 is the mean value of the input power, M2 is the mean value of the output power, M3 is the mean value of the efficiency.

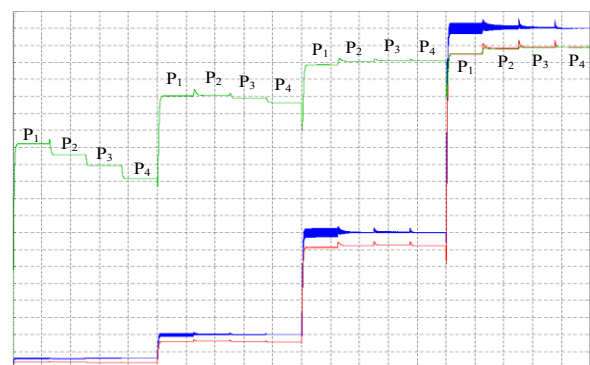


Figure 11. Results from the computer simulation, where C1: is a 5%/div efficiency (η_n): P1 is a single phase connection, P2 is a two phases connection, P3 is a three phases connection, P4 is a four phases connection, C2: is the 5W/div input power (P_{input}), C3: is the 5W/div output power (P_{output}), time is 2ms/div.

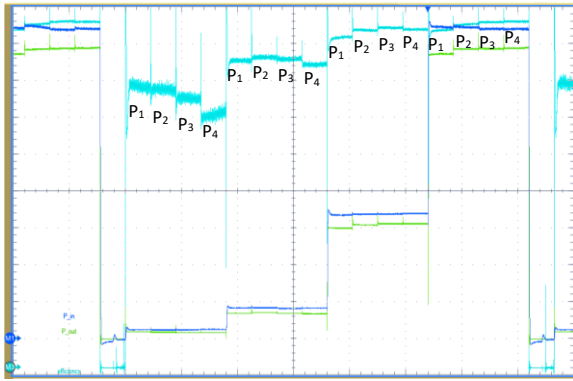


Figure 12. Experimental results: blue is the 12W/div input power (P_{input}), green is the 12W/div output power (P_{output}), light blue is the 10%/div efficiency (η_n): P1 is a single phase configuration, P2 is a two phase configuration, P3 is a three phase configuration, P4 is a four phase configuration, time is 20ms/div.

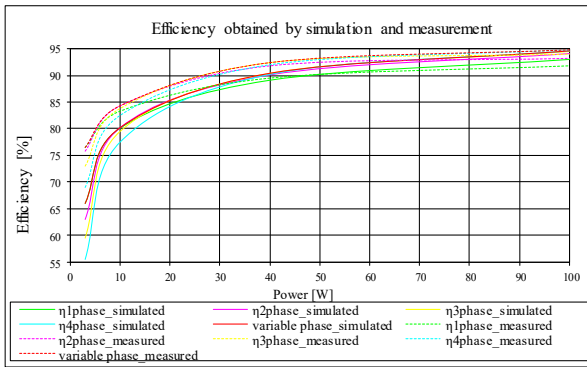


Figure 13. The graph shows the effect of power input and the number of switched phases on the efficiency of a multi-phase converter.

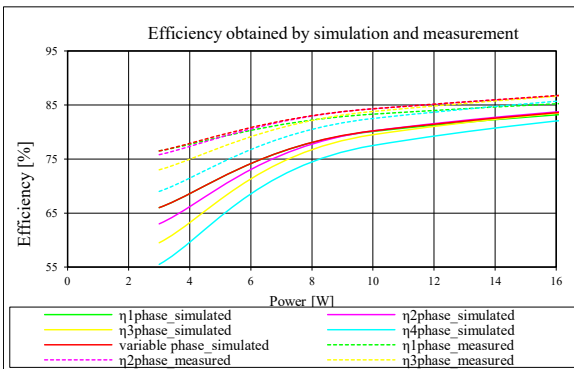


Figure 14. Relationship between the efficiency of a multi-phase converter, the power input level, and the number of active phases in a low-power input range.

Fig. 13 provides a graphical summary of the results obtained from the simulation and measurement tests. The most significant variations in the efficiency are observed at the converter lower power input levels. The phenomenon is illustrated in a greater detail in Fig. 14.

3 STRATEGY TO CONTROL THE CONVERTER TO EFFICIENCY

In practical applications of the results gained from analyzing the operation of a multi-phase buck converter, the design of its control algorithm also considers its integration with a photovoltaic panel, a common use case. To maximize the efficiency of the electric energy conversion from a photovoltaic panel, the control algorithm incorporates the maximum power point tracking (MPPT). The process relies on a microcontroller equipped with A/D converters to measure the input and output voltage and current, enabling the calculation of the input and output power and the overall efficiency of the multi-phase converter [20-22]. Notably, operating all the converter phases simultaneously may not always be efficient due to the associated losses, as observed in analysis, simulations,

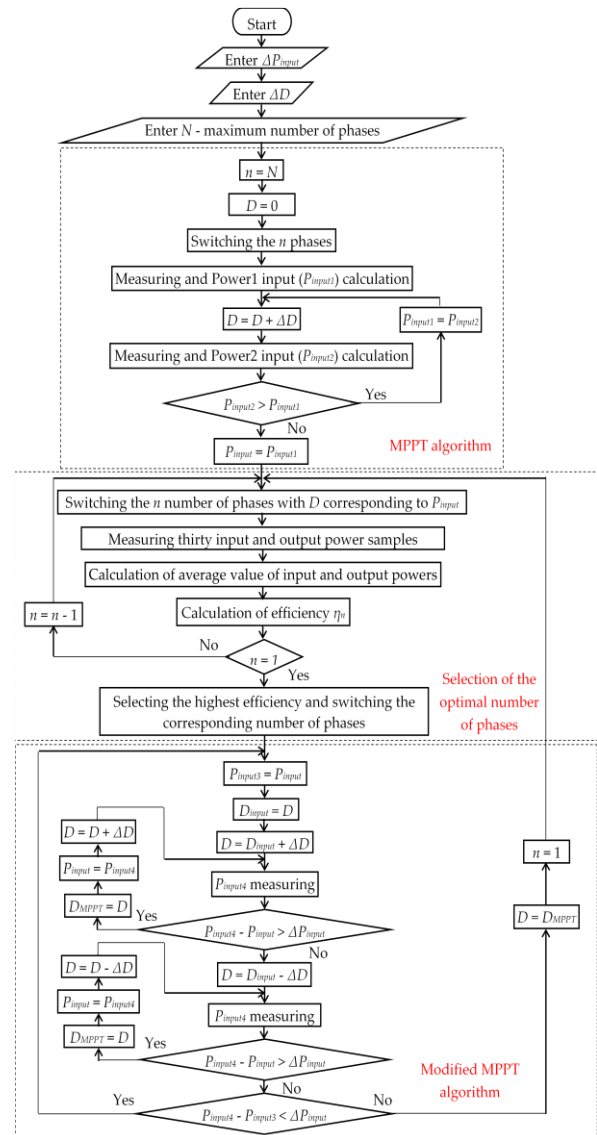


Figure 15. Flowchart illustrating the control process for a multi-phase converter.

and experimental measurements. Consequently, an adaptive topology is employed, activating only an optimal number of switching phases to minimize the losses. The approach is outlined in the flowchart in Figure 15.

The efficiency optimization control algorithm comprises three stages. First, the maximum power point (MPP) of the photovoltaic source is determined using the hill climbing method. The algorithm then identifies the optimal number of the active phases in the converter that yields the highest efficiency. This is achieved by incrementally reducing the number of the active phases, measuring the input and output power, and calculating the corresponding efficiency. The algorithm now evaluates whether there has been a significant change in the input power. If a substantial change is detected, the algorithm recalculates the optimal number of the active phases for the new input power level. Conversely, if there is no significant change in the input power observed, the algorithm maintains current duty cycle D and the phase configuration.

4 MEASUREMENT RESULTS

The algorithm is implemented using the circuit shown in Fig 5. The measurement results are given in Figs. 16-18. They show the relationship between the efficiency, the

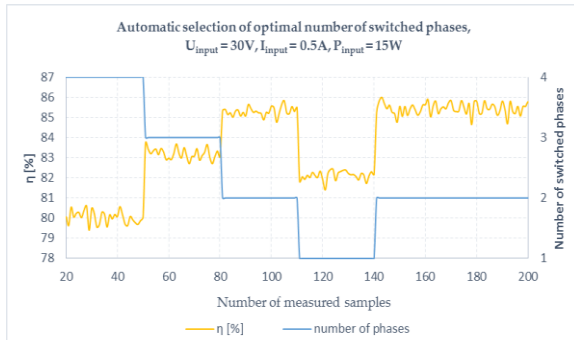


Figure 16. Measurements performed on a four-phase buck converter utilizing the proposed algorithm at the 15W input power.

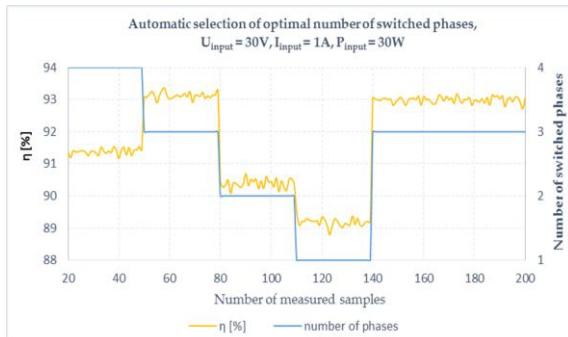


Figure 17. Measurements performed on a four-phase buck converter utilizing the proposed algorithm at the 30W input power.

number of the inverter switching phases and the number of samples processed by the microcontroller. The

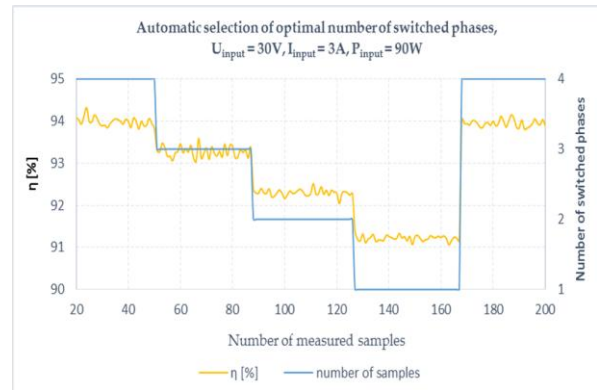


Figure 18. Measurements performed on a four-phase buck converter utilizing the proposed algorithm at the 90W input power.

performance of the microcontroller plays a crucial role in the accurate implementation of the control algorithm. For an optimal determination of the number of the switching phases, the efficiency is measured and recorded 30 times for each given topology, thereby minimizing potential measurement errors. For a four-phase converter, 120 samples are measured and analyzed. With a moderately powerful microcontroller, the entire process typically takes several hundred microseconds.

The presented control method for a multi-phase buck converter integrated with a photovoltaic panel offers favourable advantages. It is particularly effective in real-world applications where the intensity of the light radiation fluctuates significantly due to varying weather conditions and seasonal changes.

5 CONCLUSION

From Figures 12 and 13 and 16 to 18, two important key conclusions can be drawn. First, the implemented control algorithm proves effective in improving the efficiency of the photovoltaic energy conversion by 5-10% at lower power levels and by 3% at higher power levels. Such efficiency increase is particularly noteworthy during winter when the solar radiation intensity is reduced. Second, the impact of individual component parameters in the multi-phase converter is substantial, as proven by the discrepancy between the simulation and measurement results. A major advantage of the proposed control method is that most of the existing photovoltaic systems already incorporate microprocessors for system management, thus enables an immediate application of the method by modifying only the software necessitating no significant hardware changes, thereby facilitating a substantial energy saving.

REFERENCES

- [1] K. T. Hafeez et al., "A low-cost multi-phase 3A buck converter with improved ripple cancellation for wide supply range", IEEE ISCAS, 2016, pp. 1618-1621.

- [2] Y. S. Roh et al., "A multiphase synchronous buck converter with a fully integrated current balancing scheme", *IEEE Transactions on Power Electronics*, vol. 30, (2015), pp. 5159 – 5169.
- [3] P. Azer, A. Emadi, "Generalized State Space Average Model for Multi-Phase Interleaved Buck, Boost and Buck-Boost DC-DC Converters: Transient, Steady-State and Switching Dynamics", *IEEE Access*, vol. 8, pp. 77735-77745, 2020, doi: 10.1109/ACCESS.2020.2987277.
- [4] L. Wang, D. Zhang, J. Duan, R. Gu, "Research on High-Performance Multiphase DC-DC Converter Applied to Distributed Electric Propulsion Aircraft", *IEEE Transactions on Transportation Electrification*, vol. 9, no. 3, pp. 3545-3563, Sept. 2023, doi: 10.1109/TTE.2022.3207142.
- [5] M. A. Alharbi, M. S. A. Dahidah, S. A. Ali, S. A. E. Ethni, V. Pickert, "Ripple-Free Multiphase Interleaved Stacked Converter for High-Power Applications", *IEEE Transactions on Power Electronics*, vol. 37, no. 12, pp. 14770-14780, Dec. 2022, doi: 10.1109/TPEL.2022.3194979.
- [6] M. N. Rahman, D. Farrakhov, V. Vavilov, "Designing of Variable Input Multiphase Buck Converter with Efficient Phase Current Balancing Technique", in *Proc. 2023 International Conference on Electromechanical and Energy Systems (SIELMEN)*, Craiova, Romania, 2023, pp. 1-6, doi: 10.1109/SIELMEN59038.2023.10290792.
- [7] V. H. Nguyen, X. -D. Do, Y. Blaqui re, G. Cowan, "Multi-Phase Hybrid Boost Converter with High Conduction Loss Reduction and Fast Dynamic Response for Automotive Applications", in *Proc. 2022 20th IEEE Interregional NEWCAS Conference (NEWCAS)*, Quebec City, QC, Canada, 2022, pp. 183-187, doi: 10.1109/NEWCAS52662.2022.9842223.
- [8] J. Tang, T. Guo, J. S. Kim, J. Roh, "A Current-Mode Four-Phase Synchronous Buck Converter With Dynamic Dead-Time Control", *IEEE Access*, vol. 9, pp. 81078-81088, 2021, doi: 10.1109/ACCESS.2021.3085826.
- [9] N. Hinov, T. Hranov, "Model-Based Optimisation of a Buck-Boost DC-DC Converter", in *Proc. 2020 21st International Symposium on Electrical Apparatus & Technologies (SIELA)*, Bourgas, Bulgaria, 2020, pp. 1-5, doi: 10.1109/SIELA49118.2020.9167056.
- [10] A. Kulshreshtha, A. R. Saxena, M. Veerachary, "Non-Isolated Fourth-Order Boost DC-DC Converter for Power Management in Low Voltage Low Power DC Grids: Design and Interaction Analysis", *IEEE Access*, vol. 8, pp. 196500-196514, 2020, doi: 10.1109/ACCESS.2020.3034181.
- [11] J. Li, L. Zhang, X. Wu, Z. Zhou, Y. Dai, Q. Chen, "Current Estimation and Optimal Control in Multiphase DC-DC Converters With Single Current Sensor", *IEEE Transactions on Instrumentation and Measurement*, vol. 73, pp. 1-14, 2024, Art no. 9003414, doi: 10.1109/TIM.2024.3396834.
- [12] Y. Kandeel, S. O'Driscoll, C. O'Math na, M. Duffy, "Optimum Phase Count in a 5.4-W Multiphase Buck Converter Based on Output Filter Component Energies", *IEEE Transactions on Power Electronics*, vol. 38, no. 4, pp. 4909-4920, April 2023, doi: 10.1109/TPEL.2022.3226708.
- [13] Y. Lyu, B. N. Sanusi, Z. Ouyang, "Modeling and Analysis of Coupling Effect in Four Legged Core for Multi-phase Buck Converter", in *Proc. 2023 IEEE Applied Power Electronics Conference and Exposition (APEC)*, Orlando, FL, USA, 2023, pp. 3307-3313, doi: 10.1109/APEC43580.2023.10131131.
- [14] P. Jacko, M. Beres, I. Kovacova, J. Molnar, T. Vince, J. Dziak, B. Fecko, S. Gans, D. Kovac, "Remote IoT Education Laboratory for Microcontrollers Based on the STM32 Chips", *Sensors*, Vol. 22 (2022), Issue 4, pp. 1-22, doi: 10.3390/s22041440.
- [15] S. Sridhar and Q. Li, "Multiphase Constant On-Time Control With Phase Overlapping—Part I: Small-Signal Model", *IEEE Transactions on Power Electronics*, vol. 39, no. 6, pp. 6703-6720, June 2024, doi: 10.1109/TPEL.2024.3368343.
- [16] T. Golla, S. Kapat, N. Chittaragi, R. A. Setty, S. Sridharan, "Controller Design and Phase Current Balancing for Fast Dynamic Performance in Voltage Mode Controlled Multiphase Buck Converters", in *Proc. 2023 IEEE Applied Power Electronics Conference and Exposition (APEC)*, Orlando, FL, USA, 2023, pp. 2163-2169, doi: 10.1109/APEC43580.2023.10131482.
- [17] A. U. Rahman, F. Pellitteri, N. Campagna, A. O. Di Tommaso, R. Miceli, "Current Sharing Control of Multiphase Interleaving Single Inductor Four Switch Buck-Boost Converter for Energy Storage System", in *Proc. 2024 IEEE 15th International Symposium on Power Electronics for Distributed Generation Systems (PEDG)*, Luxembourg, Luxembourg, 2024, pp. 1-6, doi: 10.1109/PEDG61800.2024.10667462.
- [18] M. Duan, J. Duan, L. Sun, "Sensorless Current-Sharing Scheme for Multiphase DC-DC Boost Converters", *IEEE Transactions on Power Electronics*, vol. 38, no. 2, pp. 1398-1405, Feb. 2023, doi: 10.1109/TPEL.2022.3208890.
- [19] A. K. Gupta, M. Kumar, "Characterization and Localization of Open Circuit Faults for n-Phase Interleaved Buck Converter", *IEEE Transactions on Industry Applications*, vol. 60, no. 2, pp. 3273-3283, March-April 2024, doi: 10.1109/TIA.2023.3332053.
- [20] C. -J. Tsai, H. -H. Chen, C. -J. Chen, "A Phase Interpolated Dual-Phase Adaptive On-Time Controlled Buck Converter", *IEEE Transactions on Circuits and Systems I: Regular Papers*, vol. 71, no. 11, pp. 5155-5165, Nov. 2024, doi: 10.1109/TCSI.2024.3423439.
- [21] G. Eckhardt, J. M. Lenz, "Four-phase Buck Converter Design and Thermal Modeling Using FEA Simulation", in *Proc. 2022 14th Seminar on Power Electronics and Control (SEPOC)*, Santa Maria, Brazil, 2022, pp. 1-6, doi: 10.1109/SEPOC54972.2022.9976419.
- [22] N. Deshmukh, S. Prabhakar, S. Anand, "Power Loss Reduction in Buck Converter Based Active Power Decoupling Circuit", *IEEE Transactions on Power Electronics*, vol. 36, no. 4, pp. 4316-4325, April 2021, doi: 10.1109/TPEL.2020.3024721.

Kovac Dobroslav received his M.Sc. and Ph.D. degrees in power electronics in 1985 and 1992, respectively from the Technical University of Ko ice, the Slovak Republic. From 1985 to 1991 he worked as a researcher at the Department of Electrical Drives and from 1991 to 2000 as an assistant lecturer of the Department of Theoretical Electrical Engineering and Electrical Measurement. Since 2000, he has been a professor at the Department of Theoretical and Industrial Electrical Engineering. His research interests include practical application of advanced power semiconductor devices, computer simulations, industrial systems, smart electronics, and automated computer measurement. In recognition of his contributions to science and technology he received in 1989 the "Award of the Minister of Education for the Development of Science and Technology".

Kovacova Irena received her M.Sc. and Ph.D. degrees in power electronics in 1982 and 1988, respectively from the Technical University of Ko ice, the Slovak Republic. From 1982 to 2012 she was a member of the Department of Electrical Drives, where first worked she as an assistant lecturer and later as an associate professor. Since 2012, she has been a professor of the Department of Theoretical and Industrial Electrical Engineering. Her current professional focus is on control and power electronics, particularly the development and construction of power converters and inverters utilizing advanced components, as well as computer simulation of emerging power semiconductor parts, devices, and systems. In recognition of her contributions to science and technology, she has received the "Award of the Minister of Education for the Development of Science and Technology" in 1989.